

A Method for Grid Simulation Assessing Demand Side Management Strategies

Michael Schuler^{1,2}, Bernhard Faessler^{1,2}, Markus Preißinger^{1,2} and Peter Kepplinger^{1,2}

¹ Josef Ressel Center for Applied Scientific Computing in Energy, Finance, and Logistics, Vorarlberg University of Applied Sciences, Hochschulstraße 1, 6850 Dornbirn, Austria

² Illwerke vkw Endowed Professorship for Energy Efficiency, Energy Research Center, Vorarlberg University of Applied Sciences, Hochschulstraße 1, 6850 Dornbirn, Austria
peter.kepplinger@fhv.at

Abstract. Due to the promoted integration of renewable sources, a further growth of transient and decentralized generation is expected. In addition, peak loads and an increasing demand due to electrification are presumably. Thus, the existing supply and distribution infrastructure is running the risk of reaching its physical limits. To counteract and ensure grid reliability, load management strategies are crucial. In the context of this work, a method for a grid simulation method assessing incentive driven autonomously optimized devices is presented. As an example application, differently dimensioned battery energy storage systems are integrated into a distribution grid and driven autonomously by an incentive. A rural, lightly meshed grid topology from Vorarlberg is used in combination with historic smart meter household load consumption data from the same region to evaluate the effects, on peak-to-average power ratio and voltage quality. To account for positioning effects all possible battery positions are considered. Results show that the peak-to-average ratio at the feed-in point can be improved by approx. 21 % without simultaneously worsening the voltage quality. The results also confirm that the charge and discharge power of the battery energy storage shows a higher impact on the evaluated criteria than the energy capacity.

Keywords: Grid Simulation, Autonomous Demand Side Management, Battery Energy Storage Systems.

1 Introduction

The knowledge about effects of load balancing measures by the use of controlled loads and storages in low-voltage distribution grids is limited. Beside numerous publications dealing with load flow calculations [1]–[3] and load management strategies [4]–[8], only a few publications consider both topics linked [9]–[12]. However, the behavior of the electrical grid supported by load balancing measures is of central importance to assess all possible effects. In order to predict the behavior well, the base loads at the individual nodes of the grid have to be deliberately chosen. Household loads [12] are often based on future estimates of load profiles. However, these load profiles do not determine the currently prevailing state. Several publications investigate the effects of

using electric vehicles as load balancing measure (vehicle-to-grid) [13]–[15]. The vehicle batteries cannot be used unrestrictedly for the load balancing, since they are not permanently connected to the electrical grid. Therefore, battery energy storage systems (BESSs) for load balancing is frequently discussed [16]–[21]. In these publications, different sizes and battery technologies are debated and their suitability demonstrated. In this work, a method for a grid simulation method assessing incentive driven autonomously optimized devices is presented. In this context, the simulation method should show the effects of autonomously operating loads in a low-voltage distribution grid. As an example application autonomous BESSs [29] are connected to a rural grid from Vorarlberg. Anonymized smart meter household load consumption data from the same region are used as loads and are randomly allocated to the nodes of the electrical grid. Furthermore, a single BESS is attached to the grid. The impact of the autonomous operation of a BESS with different maximum powers and capacities on the grid quality (peak-to-average power ratio (PAPR), voltage quality) is of strong interest in order to be able to answer the following two applied research questions: 1) Does autonomous load balancing of additional batteries improve or deteriorate the grid quality? 2) Which powers and capacities contribute to improvements or deterioration in grid quality? The results of the grid simulation for a given grid topology depend on a variety of selectable parameters: The allocation of household loads in the distribution grid; The battery storage positioning in the distribution grid; The maximum power and capacity of the BESS. Therefore, parameterization of the BESS and its position has been varied. In Sec. 2, the detailed grid simulation approach is presented. Sec. 3 deals with the parametrization of the electrical grid and the BESS, as well as the description of the different incentives. Furthermore, the simulation procedure is discussed and the results of the example application to BESS are shown. A brief conclusion and outlook is given in Sec. 4.

2 Method

The proposed simulation method allows simulating - in addition to arbitrary base load profiles and decentralized generation, e.g. PV feed in - incentive driven autonomously optimized devices in a low voltage distribution grid. Furthermore, it is possible to attribute temporal changes of the state of the low voltage grid to the behavior of the loads. Thus, between two consecutive time steps, a closed loop between the grid and individual loads is achieved. In the case of incentive driven devices, this can lead to another timetable of this device, because of changed input parameters for the autonomous device. Another advantage is that the simulation is able to handle any kind of grid topology.

In order to achieve this high flexibility of loads within the simulation, we have developed three interfaces. One interface initializes the individual loads and the decentralized, autonomously optimized devices. Another one determines the behavior of the autonomously optimized devices. Using the third interface, the behavior of the base loads and autonomously optimized devices can be simulated. These interfaces are embedded into a program sequence, which is presented in detail in **Fig. 1**.

The program sequence initially defines the simulation time step Δt_{grid} and the corresponding amount of time steps n_{grid} . Subsequently, the electrical grid is initialized by creating the impedance matrix \mathcal{Z} , which contains the grid topology information. After the grid has been fully determined, the loads can be linked to the individual nodes via a predefined function f_{init} . The initialization of a load is defined as follows:

$$(\mathbf{x}_0, \mathbf{p}, \mathcal{D}, \Delta t_{\text{opt}}) = f_{\text{init}}(\Delta t_{\text{grid}}, n_{\text{grid}}), \quad (1)$$

where the initialization returns the initial state vector \mathbf{x}_0 , the system parameters \mathbf{p} in a vector form, and disturbance matrix $\mathcal{D} = (\mathbf{d}_1, \dots, \mathbf{d}_{n_{\text{grid}}})$, where each column reflects a single time step Δt_{grid} of the grid simulation. Additionally, the optimization time step Δt_{opt} between subsequent optimizations of the device is determined and returned. After initializing the loads, the load flow calculation within the simulation can be executed. If the autonomous device is to be optimized at time t_i , the following optimization function f_{man} is used to determine its future operation:

$$\mathbf{u} = f_{\text{man}}(\mathbf{c}, \Delta t_c, \mathcal{X}, \mathbf{p}, \Delta t_{\text{grid}}), \quad (2)$$

where \mathbf{c} is a vector representing an incentive function, Δt_c is the corresponding time step of the incentive function, and $\mathcal{X} = (\mathbf{x}_0, \mathbf{x}_1, \dots, \mathbf{x}_{n_{\text{grid}}})$ is a matrix containing the history of the state vectors. The optimization function returns the decision function \mathbf{u} , which represents the decision states of the autonomous optimized devices in the future. Subsequently the load current and the new states of the base loads and autonomously operated devices is iteratively calculated using the simulation function f_{sim} , defined for a load as

$$(I_i, \mathbf{x}_{i+1}) = f_{\text{sim}}(u_i, \mathbf{x}_i, \mathbf{p}, \mathbf{d}_i, U_i, bP_i, \Delta t_{\text{grid}}), \quad (3)$$

where u_i represents the current decision, \mathbf{x}_i the current state of the load, \mathbf{d}_i the current disturbances of the load, U_i the current voltage at the node and bP_i the current base load of the household. The simulation function returns the current load current I_i and updated state vector \mathbf{x}_{i+1} .

The load flow calculation is based on a direct method, in which the solution can be computed directly, if loads are given [22]–[25]. Ghatak et al. [22] provides a method in which both, line grids as well as lightly meshed grids, can be calculated. This method allows for solving the load flow by a single matrix multiplication in the form of

$$\mathbf{U}_i = U_{\text{Slack}} - \mathcal{Z} \cdot \mathbf{I}_i, \quad (4)$$

where $\mathbf{I}_i = (I_1, \dots, I_{n_{\text{Load}}})$ is the current load current vector calculated by the simulation function f_{sim} , U_{Slack} is the reference voltage at the slack node, and \mathbf{U}_i is the current voltage vector, which represents the voltages at the individual nodes. However, the voltage obtained for each node influences the current of the load. Therefore, it requires several iterations of the load simulation and the load flow calculation until a stationary solution is reached. The solution is stationary if the voltage values at all nodes change

less than a predefined voltage value ΔU between two subsequent iterations. If the simulation reaches a stationary solution, the branch currents and the feed-in power are calculated. Updating the incentive function is an optionally task during the simulation. Then, the simulation proceeds for the next time step, by increasing the simulation time.

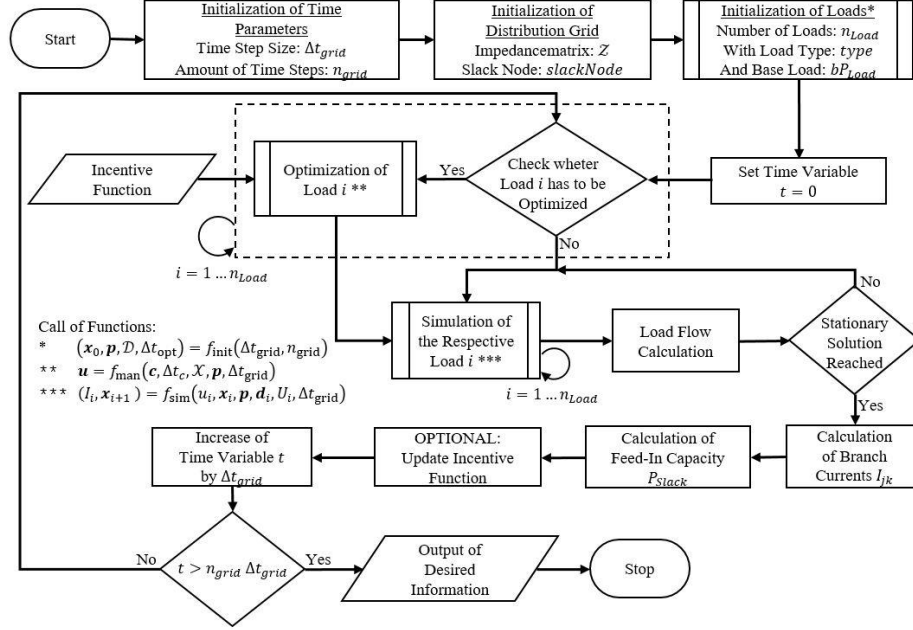


Fig. 1. Program flowchart of the grid simulation method including initialization, load flow calculation, predefined functions and time management

3 Application and Results

As an example application of the grid simulation method, the effects of integrating incentive-driven BESS on a low voltage distribution grid is evaluated. The used storage systems are operating autonomously based on an incentive, as described in detail in previous publications [26], [29]. Thereby, the study intends to show the potential of BESSs for load balancing in a low-voltage distribution grid.

3.1 Parameterization and Simulation

For a high significance of this study, real data are preferably used. The low-voltage distribution grid, cf. **Fig. 3** in the Appendix, and the household loads are based on real data from Vorarlberg. The battery storage specifications were modeled based on commercially available systems and partly modified for our investigation, cf. **Table 1** in the Appendix. All BESSs have a battery efficiency of 98 % and an AC/DC converter efficiency of 96 %. As incentive function for the battery operation, a) the Austrian day-

ahead market price for electric energy (DA) and b) the future feed-in power at the feed-in point is used (GL). The simulation is performed from 01.04.2016 00:15 to 01.09.2016 00:15 with corresponding real household loads and the Austrian day-ahead market prices.

To determine the effects of the load balancing measures, a reference simulation (Ref.) is conducted without a BESS. Then the grid simulation is extended by adding a BESS to a single grid node. The effects are evaluated. After completion, the BESS is placed to another node of the grid. This is continued until the BESS has occupied all nodes of the investigated grid. Then a different BESS from **Table 1** is selected and the effects on the grid are again determined by positioning the BESS at every node once. This is done for all BESS as presented in **Table 1** and for both incentive functions.

3.2 Results

Fig. 2 illustrates the PAPR* for selected BESSs with the same capacity, but different converter power and the two different incentives. PAPR* of all BESSs are listed in **Table 1**. Using the grid load as incentive reduces PAPR* independently of the BESS chosen. The best performing BESS (Nr. 9 in **Table 1**) with a power of 9.9 kW in **Fig. 2** shows a reduction of about 21 % compared to the reference case. The day-ahead price as incentive function increases PAPR* for all BESS parameterizations considered.

As listed in **Table 2** in the Appendix the maximum appearing voltage of BESS Nr. 9 increases by about 8 V, the minimal voltage decreases by about 4 V and 8 V by the day-ahead incentive driven and grid load incentive driven BESS, respectively. However, the overall voltage quality remains almost the same.

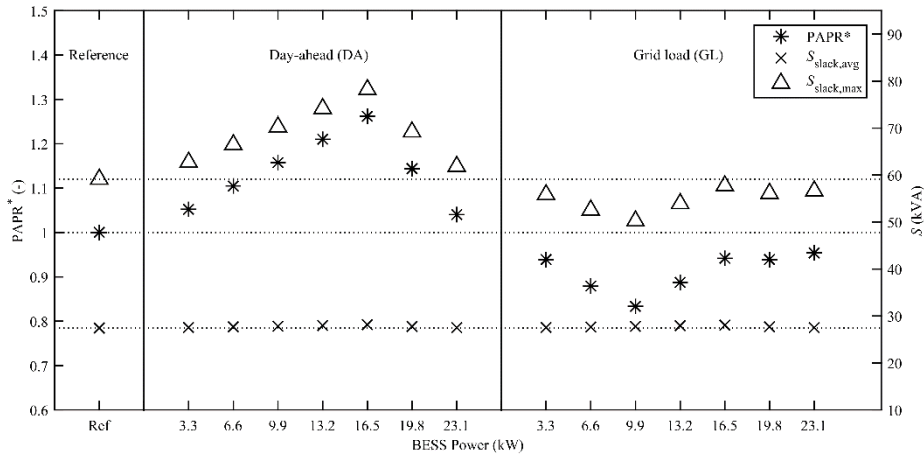


Fig. 2. Normalized peak-to-average power ratio PAPR*, average power $S_{slack,avg}$ at the slack node and maximum power $S_{slack,max}$ at the slack node for different BESSs

4 Conclusion and Outlook

A flexible grid simulation method for low-voltage distribution grids assessing demand side management driven load balancing strategies is applied to distributed, autonomously optimized devices. The knowledge of such balancing measures is limited but their behavior is of central importance since some effects can otherwise hardly be assessed. In this work a rural, weakly meshed grid section from Vorarlberg, a province in Austria is used and smart meter data from the same region, are used as household loads. Different BESSs are used as autonomously optimized devices and one is selectively attached to a node in the grid. The BESS position is varied and the effects are determined. Two incentives are considered – the Austrian day-ahead price as a global formed market driven incentive and the future grid feed-in power as local peak load compensation incentive. For the evaluation, power and voltage dependent characteristic values have been under consideration.

Results showed that the capacity of the BESS has little influence on the balancing behavior. Instead the maximum charge and discharge power of the battery is essential. The simulation showed that real-time pricing incentives, reflecting, may worsen PAPR* and therefore deteriorate the grid quality. However, PAPR* could be improved by the use of the future feed-in power as incentive. Further investigations showed that PAPR* is practically independent from the position of the BESS in the grid, because the power at the feed-in point remains the same except for minimal changes due to transmission losses. The voltage values showed that there are no significant changes in the voltage quality. Only the minimal and maximal voltages increased and decreased, respectively, because the BESS is an additional load or generator with about 84 % of the average power at the feed-in point. BESS 9 performed best with respect to PAPR*, exhibiting a capacity of 14 kWh and a maximum power of 9.9 kW, which accounts for about 36 % of the average power at the feed-in point in the reference case. The limit values of the voltage are between 217.98 V and 231.07 V, in case of optimal positioning of the BESS.

The proposed grid simulation method allows simulating time and grid dependent loads, which fulfill the given interfaces of the program. Therefore, it is possible to simulate any incentive driven loads, whose state depends on the incentive function, the current grid state and the actual time. As an outlook, autonomously optimized hot water heaters as described in [27], [28] can be tested for DSM performance. In addition, different management systems for electric vehicle charging in distribution grids can be evaluated.

Acknowledgments

The financial support by the Austrian Federal Ministry of Science, Research and Economy and the National Foundation for Research, Technology and Development is gratefully acknowledged. The simulation study conducted is based on anonymized smart meter load data provided by Vorarlberger Kraftwerke AG and real, rural grid topology data provided by Vorarlberger Energienetze GmbH.

References

1. B. Stott, "Review of load-flow calculation methods," *Proc. IEEE*, vol. 62, no. 7, pp. 916–929, 1974.
2. G. X. Luo and A. Semlyen, "Efficient load flow for large weakly meshed networks," *IEEE Trans. Power Syst.*, vol. 5, no. 4, pp. 1309–1316, Nov. 1990.
3. D. Das, D. P. Kothari, and A. Kalam, "Simple and efficient method for load flow solution of radial distribution networks," *Int. J. Electr. Power Energy Syst.*, vol. 17, no. 5, pp. 335–346, Oct. 1995.
4. L. Gelazanskas and K. A. A. Gamage, "Demand side management in smart grid: A review and proposals for future direction," *Sustain. Cities Soc.*, vol. 11, pp. 22–30, Feb. 2014.
5. G. Strbac, "Demand side management: Benefits and challenges," *Energy Policy*, vol. 36, no. 12, pp. 4419–4426, Dec. 2008.
6. P. Palensky and D. Dietrich, "Demand Side Management: Demand Response, Intelligent Energy Systems, and Smart Loads," *IEEE Trans. Ind. Inform.*, vol. 7, no. 3, pp. 381–388, Aug. 2011.
7. S. Nadel, "Utility Demand-Side Management Experience and Potential- A Critical Review," *Annu. Rev. Energy Environ.*, vol. 17, no. 1, pp. 507–535, Nov. 1992.
8. J. Aghaei and M.-I. Alizadeh, "Demand response in smart electricity grids equipped with renewable energy sources: A review," *Renew. Sustain. Energy Rev.*, vol. 18, pp. 64–72, Feb. 2013.
9. B. Hayes, I. Hernando-Gil, A. Collin, G. Harrison, and S. Djokic, "Optimal Power Flow for Maximizing Network Benefits From Demand-Side Management," *IEEE Trans. Power Syst.*, vol. 29, no. 4, pp. 1739–1747, Jul. 2014.
10. P. Siano, C. Cecati, H. Yu, and J. Kolbusz, "Real Time Operation of Smart Grids via FCN Networks and Optimal Power Flow," *IEEE Trans. Ind. Inform.*, vol. 8, no. 4, pp. 944–952, Nov. 2012.
11. M. E. T. Gerards, H. A. Toersche, G. Hoogsteen, T. van der Klauw, J. L. Hurink, and G. J. M. Smit, "Demand side management using profile steering," 2015, pp. 1–6.
12. G. Hoogsteen, A. Molderink, J. L. Hurink, and G. J. M. Smit, "Managing energy in time and space in smart grids using TRIANA," 2014, pp. 1–6.
13. P. Richardson, D. Flynn, and A. Keane, "Optimal Charging of Electric Vehicles in Low-Voltage Distribution Systems," *IEEE Trans. Power Syst.*, vol. 27, no. 1, pp. 268–279, Feb. 2012.
14. C. Pang, P. Dutta, and M. Kezunovic, "BEVs/PHEVs as Dispersed Energy Storage for V2B Uses in the Smart Grid," *IEEE Trans. Smart Grid*, vol. 3, no. 1, pp. 473–482, Mar. 2012.
15. I. Kim, "Impact of electric vehicles on peak load reduction," 2016, pp. 514–518.
16. M. Bragard, N. Soltan, S. Thomas, and R. W. De Doncker, "The Balance of Renewable Sources and User Demands in Grids: Power Electronics for Modular Battery Energy Storage Systems," *IEEE Trans. Power Electron.*, vol. 25, no. 12, pp. 3049–3056, Dec. 2010.
17. H. Qian, J. Zhang, J.-S. Lai, and W. Yu, "A high-efficiency grid-tie battery energy storage system," *IEEE Trans. Power Electron.*, vol. 26, no. 3, pp. 886–896, Mar. 2011.
18. L. Joerissen, J. Garche, C. Fabjan, and G. Tomazic, "Possible use of vanadium redox-flow batteries for energy storage in small grids and stand-alone photovoltaic systems," *J. Power Sources*, vol. 127, no. 1–2, pp. 98–104, Mar. 2004.
19. O. M. Toledo, D. Oliveira Filho, and A. S. A. C. Diniz, "Distributed photovoltaic generation and energy storage systems: A review," *Renew. Sustain. Energy Rev.*, vol. 14, no. 1, pp. 506–511, Jan. 2010.

20. R. S. Bhatia, S. P. Jain, Dinesh Kumar Jain, and B. Singh, "Battery Energy Storage System for Power Conditioning of Renewable Energy Sources," 2005, vol. 1, pp. 501–506.
21. T. Borsche, A. Ulbig, M. Koller, and G. Andersson, "Power and energy capacity requirements of storages providing frequency control reserves," 2013, pp. 1–5.
22. U. Ghatak and V. Mukherjee, "An improved load flow technique based on load current injection for modern distribution system," *Int. J. Electr. Power Energy Syst.*, vol. 84, pp. 168–181, Jan. 2017.
23. H. Li, A. Zhang, X. Shen, and J. Xu, "A load flow method for weakly meshed distribution networks using powers as flow variables," *Int. J. Electr. Power Energy Syst.*, vol. 58, pp. 291–299, Jun. 2014.
24. U. Ghatak and V. Mukherjee, "A fast and efficient load flow technique for unbalanced distribution system," *Int. J. Electr. Power Energy Syst.*, vol. 84, pp. 99–110, Jan. 2017.
25. Jen-Hao Teng, "A direct approach for distribution system load flow solutions," *IEEE Trans. Power Deliv.*, vol. 18, no. 3, pp. 882–887, Jul. 2003.
26. B. Fäßler, P. Kepplinger, M. L. Kolhe, and J. Petrasch, "Decentralized on-site optimization of a battery storage system using one-way communication," in *International Conference on Renewable Power Generation (RPG 2015)*, 2015, pp. 1–7.
27. P. Kepplinger, G. Huber, and J. Petrasch, "Autonomous optimal control for demand side management with resistive domestic hot water heaters using linear optimization," *Energy Build.*, vol. 100, pp. 50–55, Aug. 2015.
28. Kepplinger, P., Huber, G., Amann, P., Rheinberger, K., and Petrasch, J., "Active Demand Side Management with Domestic Hot Water Heaters Using Binary Integer Programming," in *e-nova 2013 Nachhaltige Gebäude Versorgung - Bewertung - Integration BAND 17*, 2013.
29. B. Faessler, P. Kepplinger, and J. Petrasch, "Decentralized price-driven grid balancing via repurposed electric vehicle batteries," *Energy*, vol. 118, pp. 446–455, Jan. 2017.

Appendix

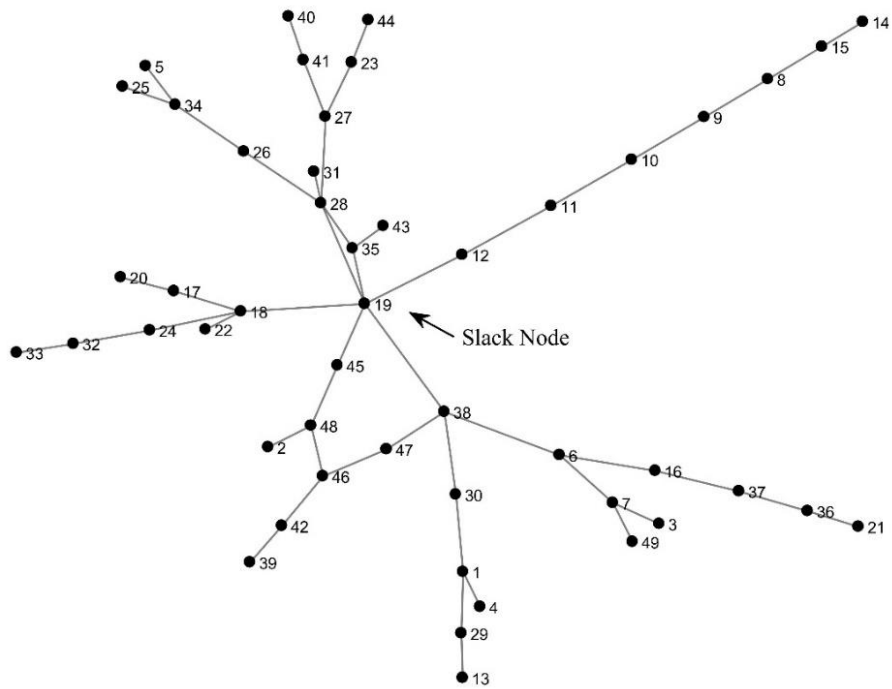


Fig. 3. Rural, lightly meshed low voltage distribution from Vorarlberg

Table 1. Power-dependent characteristic values of the different BESSs including peak-to-average power ratio PAPR, normalized peak-to-average power ratio PAPR*, average feed-in power $S_{slack,avg}$, maximum feed-in power $S_{slack,max}$ and minimum feed-in power $S_{slack,min}$. For each value, all power values at every time step are evaluated. For the incentive driven simulation (GL and DA), where the BESS is attached to each node once, all power values from each sub simulation are evaluated.

BESS	Power (kW)	Capacity (kWh)	PAPR (-)		PAPR* (-)		$S_{slack,avg}$ (kVA)		$S_{slack,max}$ (kVA)		$S_{slack,min}$ (kVA)	
			GL	DA	GL	DA	GL	DA	GL	DA	GL	DA
Ref	-	-	2.16	2.16	1.00	0.95	27.4	27.4	59.1	59.1	12.8	12.8
1	3.3	6	2.27	2.03	1.05	0.89	27.5	27.5	62.7	55.8	9.9	14.8
2	3.3	10	2.27	2.02	1.05	0.89	27.6	27.5	62.7	55.8	9.9	16.1
3	3.3	14	2.27	2.02	1.05	0.89	27.6	27.5	62.7	55.8	9.9	16.1
4	6.6	6	2.39	1.91	1.11	0.84	27.7	27.6	66.4	52.7	6.9	11.5
5	6.6	10	2.38	1.90	1.11	0.84	27.7	27.6	66.4	52.5	6.9	11.5
6	6.6	14	2.38	1.89	1.10	0.83	27.7	27.7	66.4	52.5	6.9	11.8
7	9.9	6	2.50	1.94	1.16	0.86	27.8	27.7	70.2	54.2	4.0	8.2
8	9.9	10	2.50	1.90	1.16	0.84	27.8	27.8	70.2	52.7	4.0	8.2
9	9.9	14	2.50	1.80	1.16	0.79	27.8	27.8	70.2	50.2	4.0	8.2
10	13.2	14	2.61	1.91	1.21	0.84	28.0	27.9	74.2	53.9	0.7	4.9
11	16.5	14	2.72	2.03	1.26	0.89	28.1	28.0	78.2	57.7	-2.6	1.6
12	19.8	14	2.47	2.02	1.14	0.89	27.8	27.7	69.2	56.1	4.9	9.1
13	23.1	14	2.24	2.06	1.04	0.91	27.5	27.5	61.8	56.6	10.6	15.1
14	13.2	18.7	2.47	2.03	1.15	0.89	27.7	27.7	69.2	56.1	4.8	9.1
15	16.5	23.3	2.46	1.99	1.14	0.88	27.9	27.8	69.2	55.3	4.9	9.1
16	19.8	28	2.26	2.04	1.05	0.90	27.5	27.5	62.4	56.1	10.2	15.1
17	23.1	32.7	2.27	2.02	1.05	0.89	27.6	27.5	62.7	55.8	9.9	15.1

Table 2. Voltage-dependent characteristic values of the different BESSs including the average voltage U_{avg} , the maximum voltage U_{max} , the minimum voltage U_{min} and the standard deviation of the voltage σ_U . For each value, all voltage values at each node and every time step are evaluated. For the incentive driven (GL and DA) simulation, where the BESS is attached to each node once, all voltage values from each sub simulation are evaluated.

BESS	Power (kW)	Capacity (kWh)	U_{avg} (V)		U_{max} (V)		U_{min} (V)		σ_U (V)	
			GL	DA	GL	DA	GL	DA	GL	DA
Ref	-	-	228.7	228.7	230.0	230.0	219.7	219.7	0.87	0.87
1	3.3	6	228.7	228.7	232.5	232.4	217.2	219.7	0.91	0.88
2	3.3	10	228.7	228.7	232.5	232.4	217.2	219.7	0.92	0.88
3	3.3	14	228.7	228.7	232.5	232.4	217.2	219.7	0.93	0.88
4	6.6	6	228.7	228.7	235.2	235.2	214.6	218.1	1.02	0.96
5	6.6	10	228.7	228.7	235.2	235.2	214.6	218.1	1.04	0.97
6	6.6	14	228.7	228.7	235.2	235.2	214.6	218.1	1.05	0.98
7	9.9	6	228.7	228.7	237.9	237.9	212.0	215.5	1.17	1.06
8	9.9	10	228.7	228.7	237.9	237.9	212.0	215.5	1.19	1.10
9	9.9	14	228.7	228.7	237.9	237.9	212.0	215.5	1.21	1.12
10	13.2	14	228.7	228.7	240.6	240.5	209.3	212.8	1.39	1.27
11	16.5	14	228.7	228.7	243.1	243.1	206.6	210.1	1.60	1.44
12	19.8	14	228.7	228.7	237.2	237.1	212.7	216.2	1.11	1.00
13	23.1	14	228.7	228.7	231.8	231.8	217.8	219.7	0.89	0.87
14	13.2	18.7	228.7	228.7	237.2	237.1	212.7	216.2	1.11	1.00
15	16.5	23.3	228.7	228.7	237.2	237.1	212.7	216.2	1.12	1.02
16	19.8	28	228.7	228.7	232.2	232.2	217.4	219.7	0.91	0.88
17	23.1	32.7	228.7	228.7	232.5	232.4	217.2	219.7	0.92	0.88